PAPER

Extracting 21 cm signal by frequency and angular filtering

RAA 2018 Vol. **18** No. **9**, 114(12pp) doi: 10.1088/1674–4527/18/9/114

http://www.raa-journal.org *http://iopscience.iop.org/raa*

***R**esearch in*
***A**stronomy and*
***A**strophysics*

Extracting 21 cm signal by frequency and angular filtering

Qi-Zhi Huang[1,2,3], Feng-Quan Wu[1], Reza Ansari[3] and Xuelei Chen[1,2,4]

[1] Key Laboratory of Computational Astrophysics, National Astronomical Observatories, Chinese Academy of Sciences, Beijing 100101, China; *xuelei@bao.ac.cn*
[2] School of Astronomy and Space Science, University of Chinese Academy of Sciences, Beijing 100049, China
[3] Université Paris-Sud, LAL, UMR 8607, F-91898 Orsay Cedex, France & CNRS/IN2P3, F-91405 Orsay, France
[4] Center for High Energy Physics, Peking University, Beijing 100871, China

Received 2018 April 20; accepted 2018 April 28

Abstract Extracting the neutral hydrogen (HI) signal is a great challenge for cosmological 21 cm experiments; both the astrophysical foregrounds and receiver noise are typically several orders of magnitude greater than the 21 cm signal. However, the different properties of the 21 cm signal, foreground and noise can be exploited to separate these components. The foregrounds are generally smooth or correlated over the frequency space along a line of sight (LoS), while both the 21 cm signal and noise vary stochastically along the same LoS. The foreground can be removed by filtering out the smooth component in frequency space. The receiver noise is basically uncorrelated for observations at different times, hence for surveys it is also uncorrelated in different directions, while the 21 cm signal, which traces the large scale structure, is correlated up to certain scales. In this exercise, we apply Wiener filters in frequency and angular space to extract the 21 cm signals. We found that the method works well. Inaccurate knowledge about the beam could degrade the reconstruction, but the overall result is still good, showing that the method is fairly robust.

Key words: methods: data analysis — (cosmology:) dark ages, reionization, first stars — cosmology: observations

1 INTRODUCTION

The neutral hydrogen 21 cm line is one of the most promising tools to study the observable Universe. Tomographic observation of the redshifted 21 cm line could be used to reveal the evolution of the intergalactic medium (IGM) throughout the Epoch of Reionization (EoR) (Madau et al. 1997; Ciardi & Madau 2003), and to map out the large scale structure and constrain cosmological parameters including the dark energy equation of state (Chang et al. 2008; Mao et al. 2008). In principle, it could even probe the cosmic dark age (Loeb & Zaldarriaga 2004). Compared with the cosmic microwave background (CMB), which images the Universe at the last scattering surface during the EoR, one advantage of the redshifted 21 cm tomography signal as a cosmological probe is that it provides a three dimensional (3D) map of the Universe at different redshifts, giving more information and also showing how the Universe evolved.

In recent years, a number of experiments set observation of 21 cm as one of their main scientific goals, for example experiments with existing telescopes such as the Green Bank Telescope (GBT; Chang et al. 2010; Masui et al. 2013; Switzer et al. 2013), Giant Metrewave Radio Telescope (GMRT; Paciga et al. 2011) and telescopes that are newly built or being built, such as the 21 CentiMeter Array (21CMA; Zheng et al. 2016), Tianlai (Chen 2012), Baryon acoustic oscillations In Neutral Gas Observations (BINGO; Battye et al. 2013), LOw-Frequency ARray (LOFAR; van Haarlem et al. 2013), Murchison Widefield Array (MWA; Tingay et al. 2013), Precision Array for Probing the Epoch of Re-ionization (PAPER; Parsons et al. 2010), Canadian Hydrogen

Intensity Mapping Experiment (CHIME; Bandura et al. 2014), Hydrogen Epoch of Reionization Array (HERA; DeBoer et al. 2017), Five-hundred-meter Aperture Spherical radio Telescope (FAST; Nan et al. 2011), Square Kilometre Array (SKA; Huynh & Lazio 2013), etc.

Although the redshifted 21 cm line can provide large amounts of information about cosmology, its detection is difficult. The cosmological 21 cm signal, whose brightness temperature is $\sim$0.14 mK at redshift $z\sim$0.8 (Chang et al. 2010; Masui et al. 2013), is highly contaminated by foreground emissions whose brightness temperatures are 4–5 orders of magnitude higher (de Oliveira-Costa et al. 2008; Liu & Tegmark 2012). The foregrounds at low frequency include primarily Galactic synchrotron emission which originates from cosmic ray electrons moving in the Galactic magnetic field, Galactic free-free emission which is produced by free electrons scattering off ions without being captured, and extragalactic radio sources such as radio-loud galaxies and quasars (Shaver et al. 1999; Jelić et al. 2008). Additionally, such observations are also affected by radio frequency interference (RFI) and propagation effects in the ionosphere.

Removing the foregrounds has been a big challenge in the redshifted 21 cm experiments, and a number of methods have been proposed and developed. The general idea is to exploit the different properties of foregrounds and the cosmological 21 cm signal. Along one line of sight (LoS), the cosmological 21 cm signal varies with redshift or frequency randomly, while the astrophysical foregrounds vary smoothly. The foreground can in principle be removed by LoS fitting (Wang et al. 2006; Gleser et al. 2008) or by cross-correlating data from different frequency bins (Santos et al. 2005). More recently, blind or semi-blind methods, such as the Singular Value Decomposition (SVD) method (Paciga et al. 2011; Masui et al. 2013), Robust Principal Component Analysis (Zuo et al. 2018) and Independent Component Analysis (Chapman et al. 2012; Wolz et al. 2014), have been applied.

In this paper, we introduce a simple and fast method which is based on the Wiener filter to extract the 21 cm signal. The Wiener filter has been widely used in signal processing, especially for removing noise in time series or images. We use a simulation to demonstrate our method.

The rest of this paper is structured as follows. In Section 2, we describe the Wiener filter method in general and also describe the set up for our simulation. In Section 3, we apply the method to simulated data and present the results we obtained. Finally, we discuss a number of relevant issues in the data processing and conclude in Section 4.

2 METHOD

In an HI intensity mapping survey experiment, the observed sky emission is a mixture of the 21 cm signal, noise and foregrounds. To extract the cosmologically interesting 21 cm signal, different statistical properties are used to separate them. On the relevant scale, the cosmological 21 cm signal varies stochastically, as the signal strength at each frequency corresponds to the emission of a specific redshift, and on large scales the densities at each different position are independent of each other (though there is correlation to some degree). By comparison, the foreground varies smoothly in frequency space, so it could in principle be distinguished from the 21 cm line. In addition to the sky signals, the electronic circuitry of the receiver also generates noise. After bandpass calibration, the noise could be approximated as zero-mean white noise. Based on their different properties, it is possible, at least in principle, to extract the 21 cm signal from the much stronger foregrounds and noise.

In an actual radio telescope, the data would be first pre-processed to remove bad data (e.g. those with hardware malfunction or radio frequency interference), calibrated, re-binned in frequency and time resolution, rearranged in predefined order, then used to form image cubes with two angular dimensions and one frequency dimension. These steps will depend on the particular telescope in question, e.g. the data from a single dish telescope would be processed very differently from the data collected by an interferometer array. Here, we will deal with the data processing that occurs after these steps. We will assume that an image cube has been obtained through these steps.

Below we make the 21 cm signal extraction in two steps. In the first step, we filter the data along each LoS to remove the foreground component by using their different properties. As a result, the foreground data could be significantly suppressed, while the 21 cm signal and thermal noise are kept. In the second step, we filter the data in the two dimensional (2D) angular space, to remove the randomly fluctuating noise signal, while keeping the more stable and consistent 21 cm signal.

2.1 Wiener Filter

We assume that in an experiment the observational data $\mathbf{y}$ are linearly related to $\mathbf{x}$, the physical quantity we try to measure,

$$\mathbf{y} = \mathbf{A}\,\mathbf{x} + \mathbf{n}, \tag{1}$$

where $\mathbf{A}$ is the response matrix of the system and $\mathbf{n}$ is random noise. We use boldface letters to denote vectors and matrices, and $^{\rm T}$ denotes matrix or vector transpose (we assume the data are real numbers here). The covariance matrices for the signal and noise are $\mathbf{S} = \langle \mathbf{x}\,\mathbf{x}^{\rm T}\rangle$, $\mathbf{N} = \langle \mathbf{n}\,\mathbf{n}^{\rm T}\rangle$ respectively. If $\mathbf{S}$ and $\mathbf{N}$ are known, an unbiased estimate of the signal can be obtained by applying a Wiener filter $\mathbf{W}$ to the data (Tegmark 1997),

$$\hat{\mathbf{x}} = \mathbf{W}\mathbf{y} \equiv \mathbf{S}\mathbf{A}^{\rm T}\left[\mathbf{A}\mathbf{S}\mathbf{A}^{\rm T} + \mathbf{N}\right]^{-1}\mathbf{y}. \tag{2}$$

The Wiener filter is optimal in the sense that it minimizes the variance of the estimator

$$V = \langle (\mathbf{x} - \hat{\mathbf{x}})(\mathbf{x}^{\rm T} - \hat{\mathbf{x}}^{\rm T})\rangle.$$

2.2 Simulation Setup

As the signal extraction utilizes our prior knowledge or expectation of the 21 cm signal, foreground and noise, an optimal filter depends on their statistics, so the properties of a filter also depend on the particular problem. Here we describe the basic setup we use in this exercise.

We consider the mid-redshift experiment aimed at detecting the baryon acoustic oscillation (BAO) signal of the large scale structure, such as the ongoing survey projects with GBT (Masui et al. 2013; Switzer et al. 2013), and dedicated experiments such as Tianlai (Chen 2012; Xu et al. 2015; Zhang et al. 2016a,b), CHIME (Bandura et al. 2014), BINGO (Dickinson 2014) and Hydrogen Intensity and Real-time Analysis eXperiment (HIRAX; Newburgh et al. 2016). For such projects, the (synthetic) aperture is $50 \sim 100$ m. Below, we shall consider a fiducial frequency of 800 MHz ($z = 0.7755$) and a 100 m aperture, and the corresponding full width at half maximum (FWHM) resolution is 0.25°.

We generate the 21 cm signal as follows. We adopt the Planck 2015 (Planck Collaboration et al. 2016) best fit cosmological parameters for our fiducial model. For $z = 0.7755$ the corresponding comoving angular diameter distance is $D_A = 1068.95\,{\rm Mpc}\,h^{-1}$. We consider a frequency resolution of 0.1 MHz, corresponding to a comoving radial distance interval of $\Delta D_c = 0.43\,{\rm Mpc}\,h^{-1}$ at this redshift. For our 21 cm simulation, we generate an image cube with 200^3 voxels, which is convenient for computation. Then the frequency interval is 20 MHz, i.e. $790 \sim 810$ MHz. The corresponding angular size per pixel is $\Delta\theta = \Delta D_c/D_A = 0.023^\circ$, smaller than the beam FWHM, which is good as our computation precision would not be affected by too large pixel sizes. The whole box has an angular area of $4.6^\circ \times 4.6^\circ$. The volume of the corresponding 3D box in real space is $V = L^3 = (86\,{\rm Mpc}\,h^{-1})^3$.

We assume a thermal noise with $\sigma_n = 200$ mK per voxel, which is $\sim 10^3$ times the 21 cm fluctuation of $\sim$0.2 mK in our frequency (redshift) range. Note that the beam area is about 10^2 times larger than the pixel area, so if the noise from different pixels is independent of each other, this corresponds to a noise level of $\sigma_T = 20$ mK per beam. Note that using the measurement equation

$$\sigma_T \sim \frac{T_{\rm sys}}{\eta\sqrt{\Delta\nu t}}, \tag{3}$$

where $\eta < 1$ is the efficiency of the system and taking $\Delta\nu = 0.1$ MHz. If the system is stable with a typical system temperature of $T_{\rm sys} = 20\,{\rm K} \sim 100\,{\rm K}$ and the noise is thermal, this level of noise can be achieved with a few minutes of integration time. However, in real telescopes there might be a noise floor of non-thermal origin preventing the noise from reaching the low thermal value given by Equation (3) no matter how long the integration time is, so the actual noise might be higher.

Assuming the neutral hydrogen evolution is linear on the relevant scales, the dark matter power spectrum is shown in Figure 1. We then generate a random density distribution in the simulation box according to the power spectrum. Adopting an HI bias of $b_{\rm HI} = 0.70$ and HI density ratio $\Omega_{\rm HI} = 6.6 \times 10^{-4}$ (Chang et al. 2010; Masui et al. 2013), the average brightness temperature of the 21 cm signal around z∼0.8 is given by

$$\bar{T}_{21} \approx 0.284\left(\frac{\Omega_{\rm HI}}{10^{-3}}\right)\left(\frac{h}{0.73}\right)\left(\frac{1+z}{1.8}\right)^{1/2} \times \left(\frac{\Omega_m + \Omega_\Lambda(1+z)^{-3}}{0.37}\right)^{-1/2}\ {\rm mK}. \tag{4}$$

The simulated 21 cm fluctuation temperature map with $\delta T_{21}(\boldsymbol{x}) = b_{\rm HI}\bar{T}_{21}\delta(\boldsymbol{x})$ is shown in the top panel of Figure 2. We also produce a map convolved with a Gaussian beam whose FWHM resolution is 0.25°, corresponding to the resolution of a telescope with an aperture of ~ 100 m at 800 MHz frequency; this is shown in the bottom panel of Figure 2.

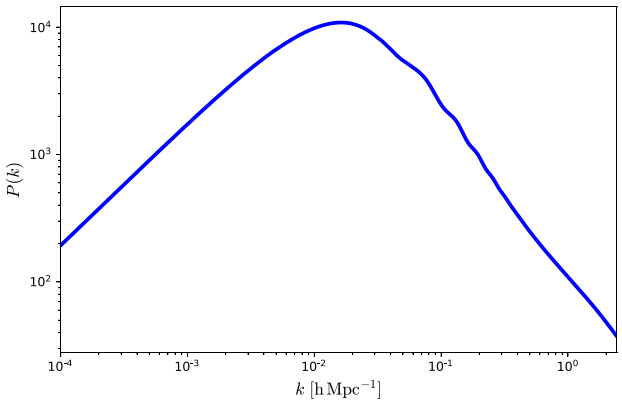

Fig. 1 Power spectrum of dark matter at $z = 0.7755$ (with non-linear correction).

We also include a few simple foreground models in the simulation. At the low frequencies, we consider three kinds of spectral indices of diffuse foreground: the Galactic synchrotron emission which dominates the low-frequency sky; a slightly more sophisticated model with frequency-varying index; multiple indices which are likely to be produced by additional components such as synchrotron emission, free-free emission, etc. In the simplest case, the brightness temperature of the foreground component is modeled with a single spectral index,

$$f(\nu) = A_* \left(\frac{\nu}{\nu_*}\right)^{\beta_*}. \tag{5}$$

We adopt $A_* = 5.3\,\mathrm{K}$, the average temperature of foreground at 800 MHz (Zheng et al. 2017) and $\beta_* = -2.76$ (Reich & Reich 1988; Testori et al. 2001). A slight improvement is to consider a running index foreground given by Wang et al. (2006)

$$f(\nu) = A_* \left(\frac{\nu}{\nu_*}\right)^{\beta_* - 0.1\ln(\nu/\nu_*)}. \tag{6}$$

Finally, for a foreground with multiple indices

$$\begin{aligned} f(\nu) =& 5.3 \left(\frac{\nu}{\nu_*}\right)^{-2.76} + 0.2 \left(\frac{\nu}{\nu_*}\right)^{-2.1} \\ &+ 0.1 \left(\frac{\nu}{\nu_*}\right)^{-3.2}. \end{aligned} \tag{7}$$

In Figure 3, we show the input 21 cm signal along one LoS in the top panel, and the total temperature including the 21 cm signal, the foreground (a single power index component) and randomly generated noise in the bottom panel.

3 RESULTS

Here we apply this method to extraction of the 21 cm signal from the observational data with foreground and noise. In the present paper, we shall adopt a two step procedure: in the first step, we process the data cube along each LoS by removing the smoothly distributed foreground component. In the second step, we apply the Wiener filter in the 2D angular space, which reduces the noise significantly to recover the 21 cm signal.

3.1 Frequency Filtering

In frequency space, for the relatively low resolution (0.1 MHz) required for intensity mapping, we may neglect the small side lobes in the frequency channels and take $\mathbf{A} = \mathbf{I}$, where $\mathbf{I}$ is the identity matrix. We rewrite Equation (1) as

$$y(\nu) = f(\nu) + s(\nu) + n(\nu), \tag{8}$$

where $f(\nu)$ is the foreground, $s(\nu)$ is the 21 cm signal and $n(\nu)$ is the noise, which we assume to be white noise with zero mean. We assume the signal, foreground and noise are uncorrelated with each other, so that $\langle (\boldsymbol{f}+\boldsymbol{s}+\boldsymbol{n})\,(\boldsymbol{f}+\boldsymbol{s}+\boldsymbol{n})^{\mathrm{T}}\rangle = \mathbf{F}+\mathbf{S}+\mathbf{N}$, where $\mathbf{S} = \langle \boldsymbol{s}\boldsymbol{s}^{\mathrm{T}}\rangle$, $\mathbf{F} = \langle f\boldsymbol{f}^{\mathrm{T}}\rangle$ and $\mathbf{N} = \langle \mathbf{n}\boldsymbol{n}^{\mathrm{T}}\rangle$.

Along one LoS, both the 21 cm signal and noise are stochastically varying on the relevant scales, while the foreground is smoother, so here we may use this to extract the foreground from the data first. If we ignore the slight imperfections in frequency channels which are fairly small, so that the response can be treated as a δ function, the foreground extraction filter is defined by

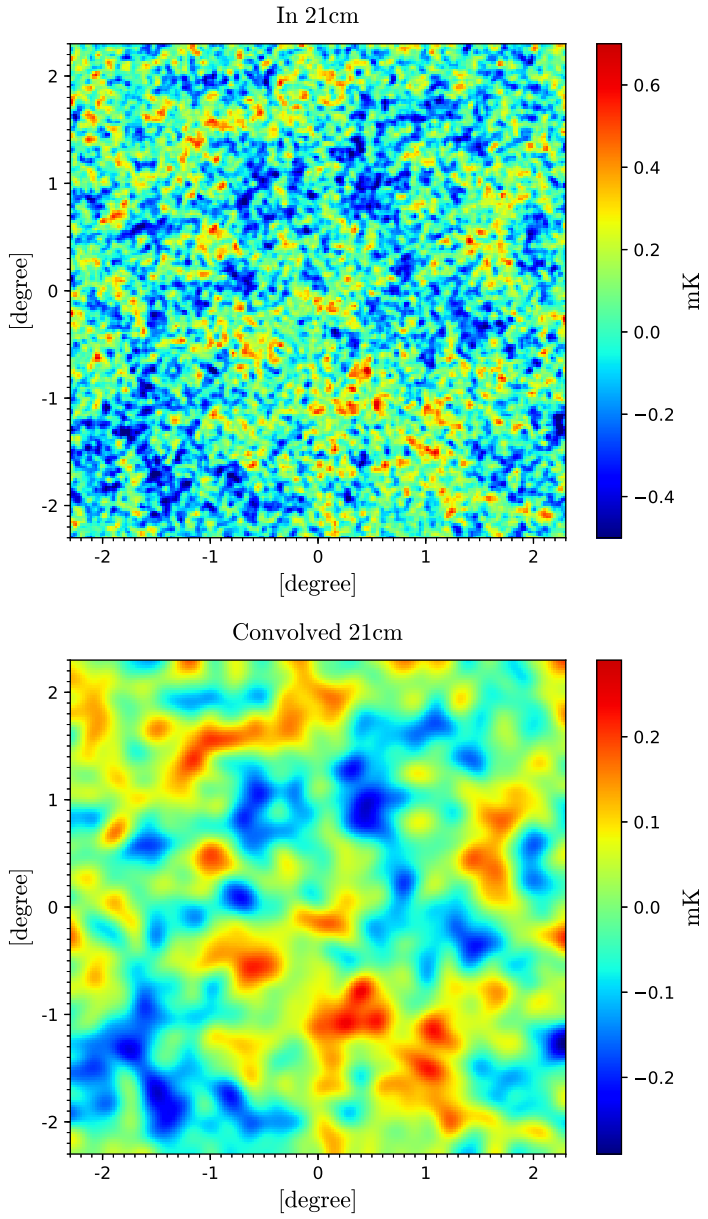

Fig. 2 *Top*: the simulated 21 cm signal at 800 MHz; *bottom*: the 21 cm signal convolved with an FWHM 0.25° Gaussian beam.

$\mathbf{W}_\nu^f = \mathbf{F}[\mathbf{F}+\mathbf{S}+\mathbf{N}]^{-1}$, while the signal+noise is described by $\mathbf{W}_\nu = \mathbf{I} - \mathbf{W}_\nu^f$.

We note that in the real world, the foreground is unknown, so strictly speaking the Wiener filter method cannot be applied. Nevertheless, the foreground is believed to be smooth in frequency space, so that even though the Wiener filter constructed this way is not very precise, it could still serve as a low-pass filter to extract the smooth component of the data. In fact, we also tried applying a simple low-pass filter and found the result is practically the same.

The filtered data $\mathbf{W}^f\mathbf{y}$ and $[\mathbf{I}-\mathbf{W}^f]\,\mathbf{y}$ are shown for a random LoS in Figure 4. From top to bottom, the three panels show the result for the single index, varying index and multi-component cases respectively. The smoothly varying and stochastically varying components are separated, but the 21 cm signal is still mixed with the noise.

3.2 Angular Space Filtering

We apply angular space filtering to separate the 21 cm signal from noise. To simplify the notation, we will omit

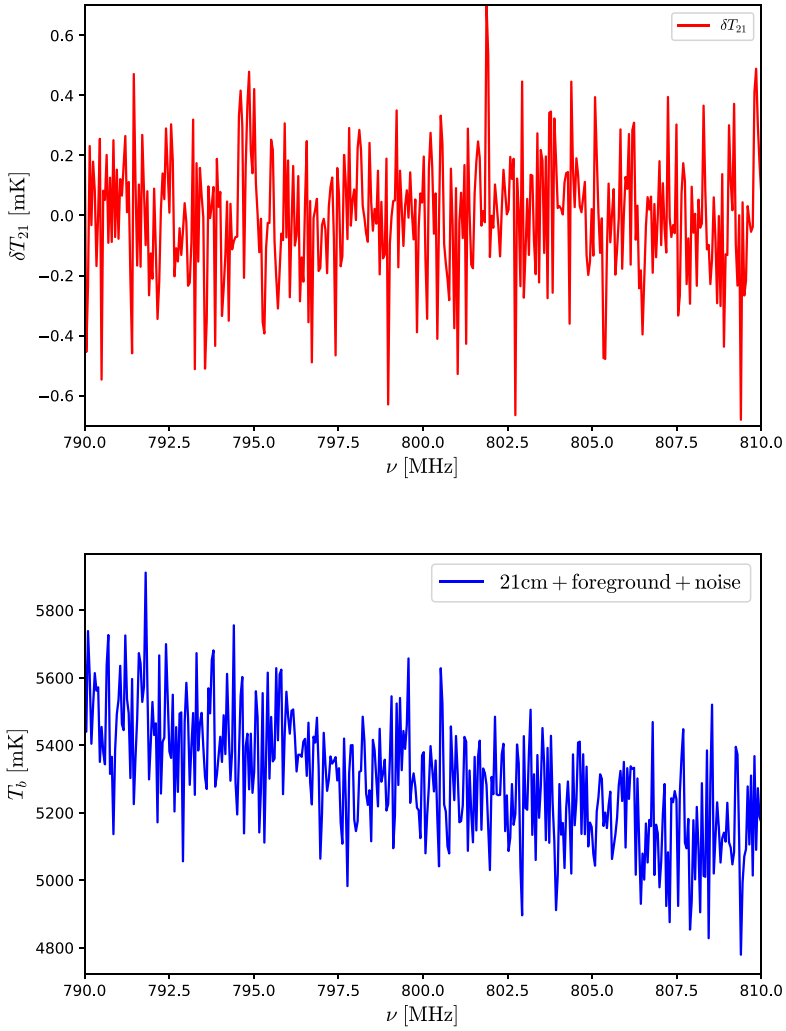

Fig. 3 The input spectrum along one LoS. *Top*: the input 21 cm signal; *Bottom*: 21 cm signal + single index foreground + noise.

the frequency variable ν in the expressions provided below, though it should be understood that all the observables and beams are functions of ν.

We label the pixels of the sky with the angular position $\boldsymbol{\theta}$, then the Gaussian beam response $\mathbf{A}$ is described by

$$A_{\boldsymbol{\theta},\boldsymbol{\theta}'} = \frac{1}{\sqrt{2\pi}\sigma_\theta} e^{-|\boldsymbol{\theta}-\boldsymbol{\theta}'|^2/(2\sigma_\theta^2)}. \quad (9)$$

The covariance matrix $\mathbf{S}$ is defined by the angular correlation function of the signal

$$\mathbf{S}_{\boldsymbol{\theta},\boldsymbol{\theta}'} = \langle T_{21}(\boldsymbol{\theta}) T_{21}(\boldsymbol{\theta}')\rangle = C(|\boldsymbol{\theta}-\boldsymbol{\theta}'|). \quad (10)$$

Here we have assumed that the 21 cm signal is statistically isotropic and homogeneous, i.e. the statistics do not depend on the position in the sky or the direction $\boldsymbol{\theta}-\boldsymbol{\theta}'$.

Expanding in spherical harmonics, we have

$$T(\boldsymbol{\theta}) = \sum_{l,m} a_{l,m} Y_{l,m}(\boldsymbol{\theta}). \quad (11)$$

Substituting Equation (11) into Equation (10) and using the relation $\langle a_{l,m} a^*_{l',m'}\rangle = C_l \delta_{l,l'}\delta_{m,m'}$, we obtain

$$C(|\boldsymbol{\theta}-\boldsymbol{\theta}'|) = \sum_{l,m} C_l Y_{l,m}(\boldsymbol{\theta}) Y^*_{l,m}(\boldsymbol{\theta}'). \quad (12)$$

Applying the addition theorem for spherical harmonics

$$\sum_{m=-l}^{l} Y_{l,m}(\boldsymbol{\theta}) Y^*_{l,m}(\boldsymbol{\theta}') = \frac{2l+1}{4\pi} P_l(\boldsymbol{\theta}\cdot\boldsymbol{\theta}'),$$

where P_l is the Legendre polynomial of l-th order, and $\boldsymbol{\theta}\cdot\boldsymbol{\theta}' = \cos\theta$ where θ is used to denote the angle between

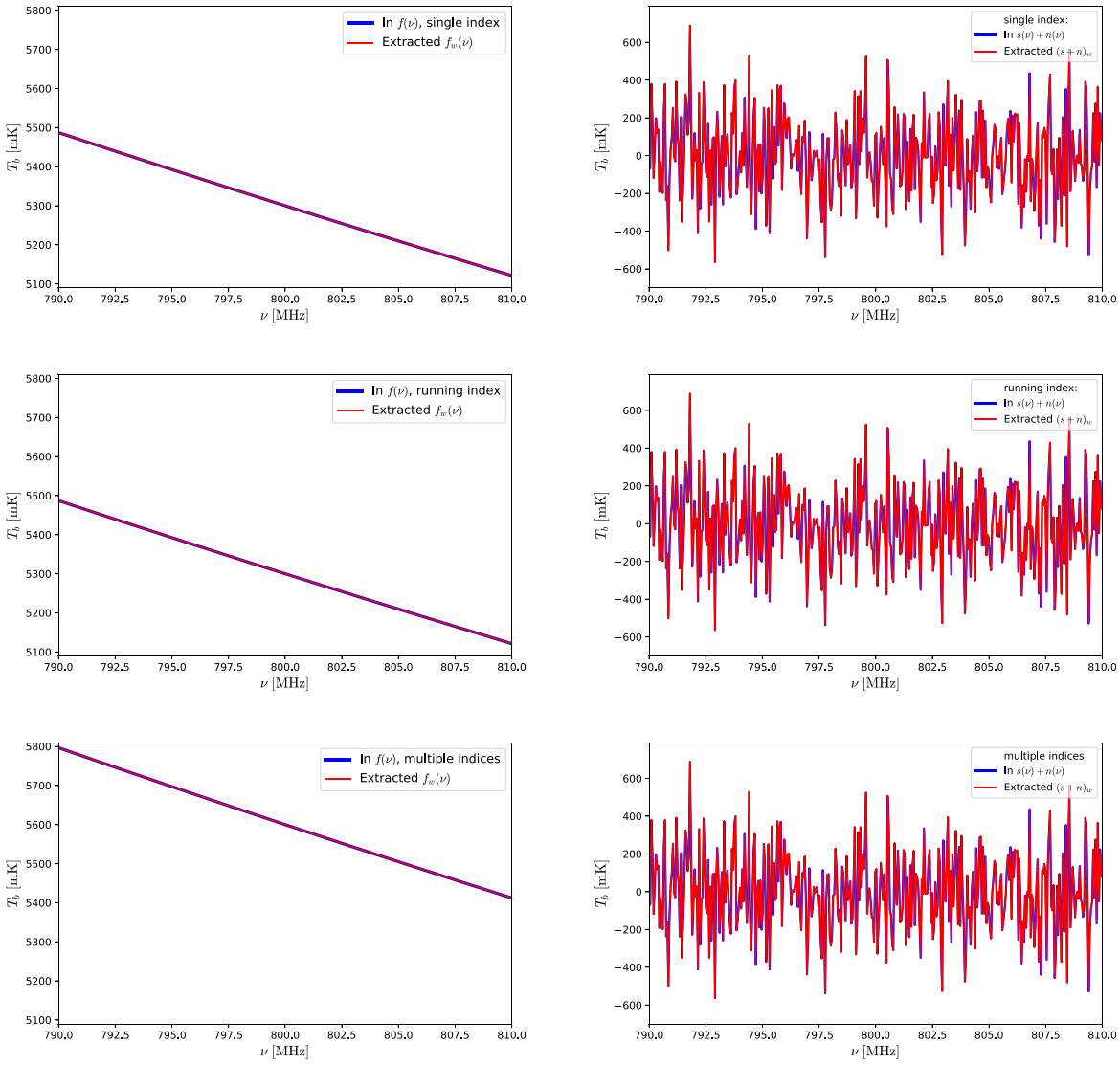

Fig. 4 *Left*: extracted foregrounds ($\mathbf{W}^f\,\mathbf{y}$). *Right*: extracted 21 cm+noise ($[\mathbf{I}-\mathbf{W}^f]\,\mathbf{y}$). *Top to bottom*: different foreground models with single index, running index and multiple indices respectively.

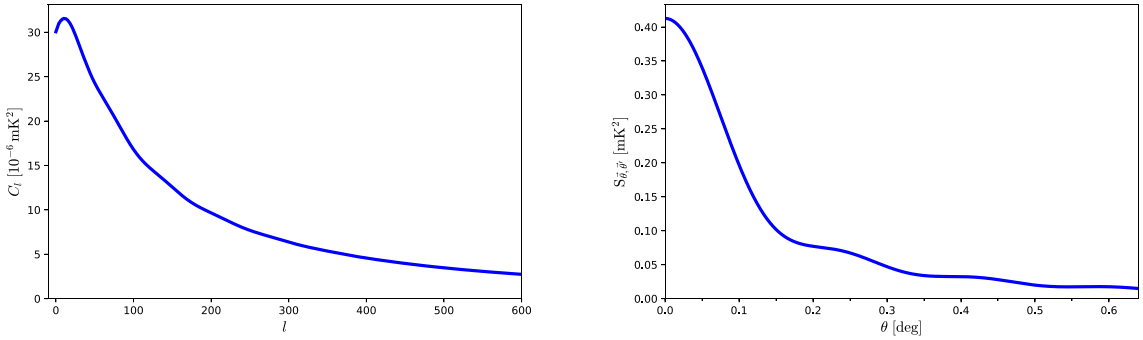

Fig. 5 C_l (*left*) and $C(\theta)$ (*right*) of 21 cm signal at $z \sim 0.8$.

the unit vectors $\boldsymbol{\theta}$ and $\boldsymbol{\theta}'$, we finally obtain

$$\mathbf{S}_{\boldsymbol{\theta},\boldsymbol{\theta}'} = \sum_l \frac{2l+1}{4\pi} C_l \, P_l(\cos\theta). \tag{13}$$

C_l can be computed from the power spectrum by considering its projection on a thin shell with bandwidth $\Delta\nu$ (Santos et al. 2005),

$$C_l(\nu) = \frac{2\Delta\nu^2}{\pi} \int k^2 dk P_{21}(k,\nu) j_l^2[kr(\nu)]. \tag{14}$$

In Figure 5 we show the angular power spectrum C_l (top panel) and corresponding angular correlation function $C(\theta)$ (bottom) panel. The correlation between 21 cm signal drops rapidly at $l \sim 10^2$ or on the degree scale.

The noise covariance matrix for pixels $\boldsymbol{\theta}, \boldsymbol{\theta}'$ is given by

$$\mathbf{N}_{\boldsymbol{\theta},\boldsymbol{\theta}'} = N_0 \delta_{\boldsymbol{\theta},\boldsymbol{\theta}'}, \tag{15}$$

where for simplicity we have assumed a constant noise N_0. Note that in Equation (1), if the vector $\mathbf{x}$ represents sky pixels while $\mathbf{y}$ corresponds to time-ordered data, then the different elements of $\mathbf{n}$ are data taken at different times and may be considered independent random samples, so the noise matrix $\mathbf{N}$ is diagonal. If we use pixels finer than the beam size, then when we re-bin the time-ordered data into sky pixels, the noise in adjacent pixels with angular distance smaller than the beam size would be correlated; this is automatically taken into account in the Wiener filter, described in Equation (2), by the response matrix $\mathbf{A}$ and $\mathbf{A}^{\mathrm{T}}$. In the real world, the noise may be more complicated, for example, the noise level may be direction-dependent, either due to brighter sky temperature or because of the operating condition of the telescope receiver. Furthermore, even the data taken at different times may have some correlation due to the presence of $1/f$ noise. These effects can also be handled by the Wiener filtering algorithm, if the noise covariance matrix $\mathbf{N}$ is known. In the present work we shall assume the simple case where the noise is uncorrelated and constant.

Figure 6 shows the extracted 21 cm map by applying the Wiener filter. From top to bottom, we plot the input map with the 21 cm signal plus 200 mK noise, the extracted 21 cm map, and the difference between the extracted map and the input map. Despite the high noise level, the 21 cm signal is successfully recovered; the difference between the recovered map and the original one is very small. Note that the Wiener filter is obtained by using the angular correlation function computed from the cosmological model, which corresponds to the ensemble average value; the actual realization may differ slightly due to sample variance, so the recovery would not be perfect.

In fact, the method could also work reasonably well even if the noise level is still higher. This is depicted in Figure 7, where the noise is assumed to be 2000 mK. Here we see that the difference between the recovered 21 cm map and the original one is larger than in Figure 6, but the overall structure of the 21 cm intensity is still clearly seen, and the difference between the two maps is still much smaller than the 21 cm brightness temperature.

In Figure 8 we display the recovered 21 cm power spectrum and relative error. The error bars are estimated from the variance in k-space. The error obtained here is for the simulation box which is $(86\,\mathrm{Mpc}\,h^{-1})^3$. If we assume that the relative error scales simply as $\Delta P/P \sim V^{-1/2}$, we estimate that in order to achieve 1% statistical precision on the power spectrum at $k = 0.1\,h\,\mathrm{Mpc}^{-1}$, the required survey volume is $(370\,\mathrm{Mpc}\,h^{-1})^3$. The actual error may be larger when sampling variance and imperfection in reconstruction are taken into account.

When making the map, the Wiener filter automatically deconvolves the data. In the above analysis the beam is assumed to be perfectly known, so the recovery is very accurate even when noise is present. Indeed, some finer details whose scales are smaller than that of the beam width are recovered in the reconstructed map, which shows the power of the Wiener filter method. However, in the real world the beam is only known either by electromagnetic field simulation or by calibration measurements, and both approaches have errors. We make a simple demonstration of the effect of an inaccurately known beam by the following exercise: we assume the real beam is a Gaussian with a beam width (FWHM) of 0.25°, but then in the reconstruction we use Gaussian beams with slightly different beam widths.

The result is shown in Figure 9. The top panels display the original 21 cm signal (top left, same as the top panel of Fig. 2) and the reconstructed map with the correct beam size (top right, same as the middle panel of Fig. 6); we put these here again for easy comparison. The bottom panels depict the reconstructed map with Gaussian beams having incorrect beam widths of 0.23° (bottom left) and 0.20° (bottom right). We see that when incorrect beam widths are used, the whole reconstructed map becomes "fuzzier" and the finer details of the original maps are lost, though the overall large scale structure

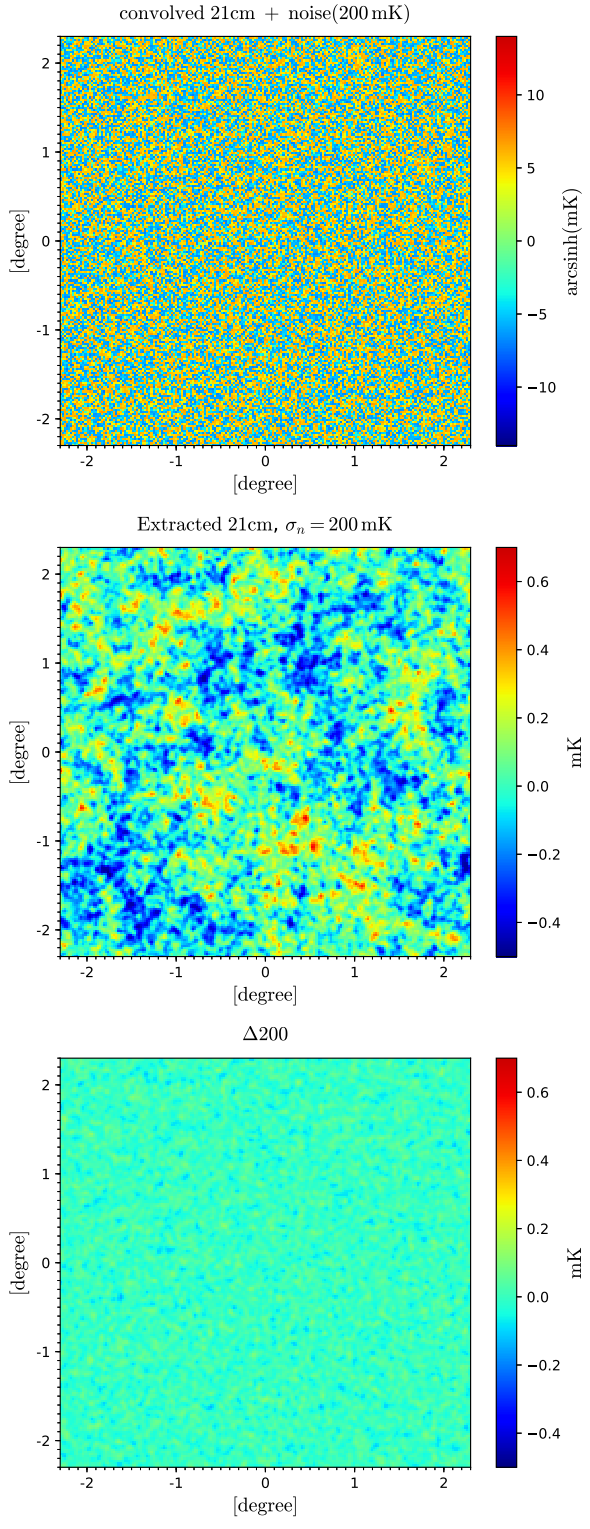

Fig. 6 *Top Panel*: 21 cm map + noise; *Middle Panel*: extracted 21 cm map; *Bottom*: difference between the extracted and input 21 cm maps.

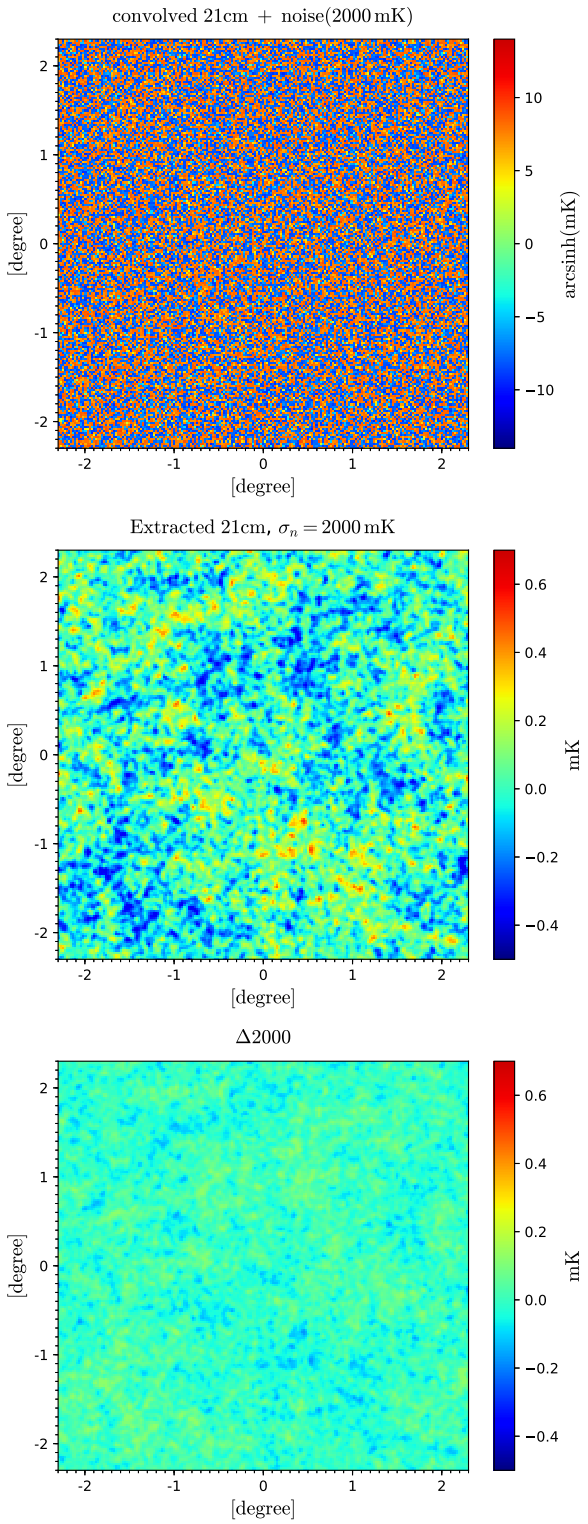

Fig. 7 Same as Fig. 6, but with higher noise level (2000 mK).

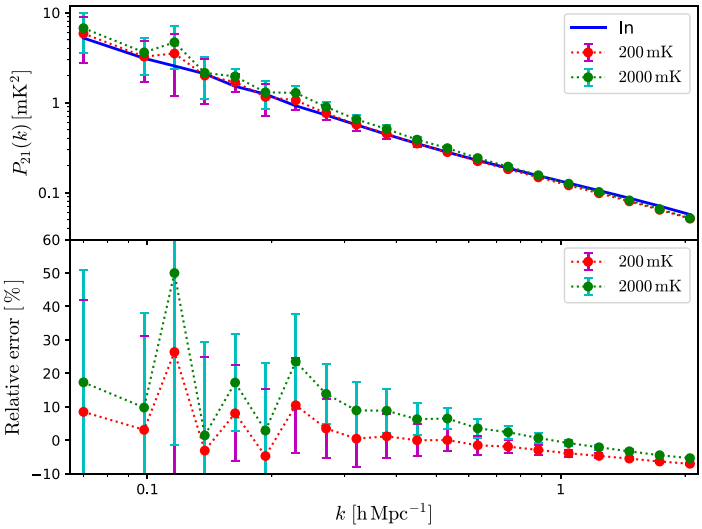

Fig. 8 The recovered 21 cm power spectrum (*top panel*) and relative error (*bottom panel*) for this simulation box. We show the power for the original (*blue line*) signal, the reconstruction with 200 mK noise (*red symbols*) and that with 2000 mK noise (*green symbols*) in the figure.

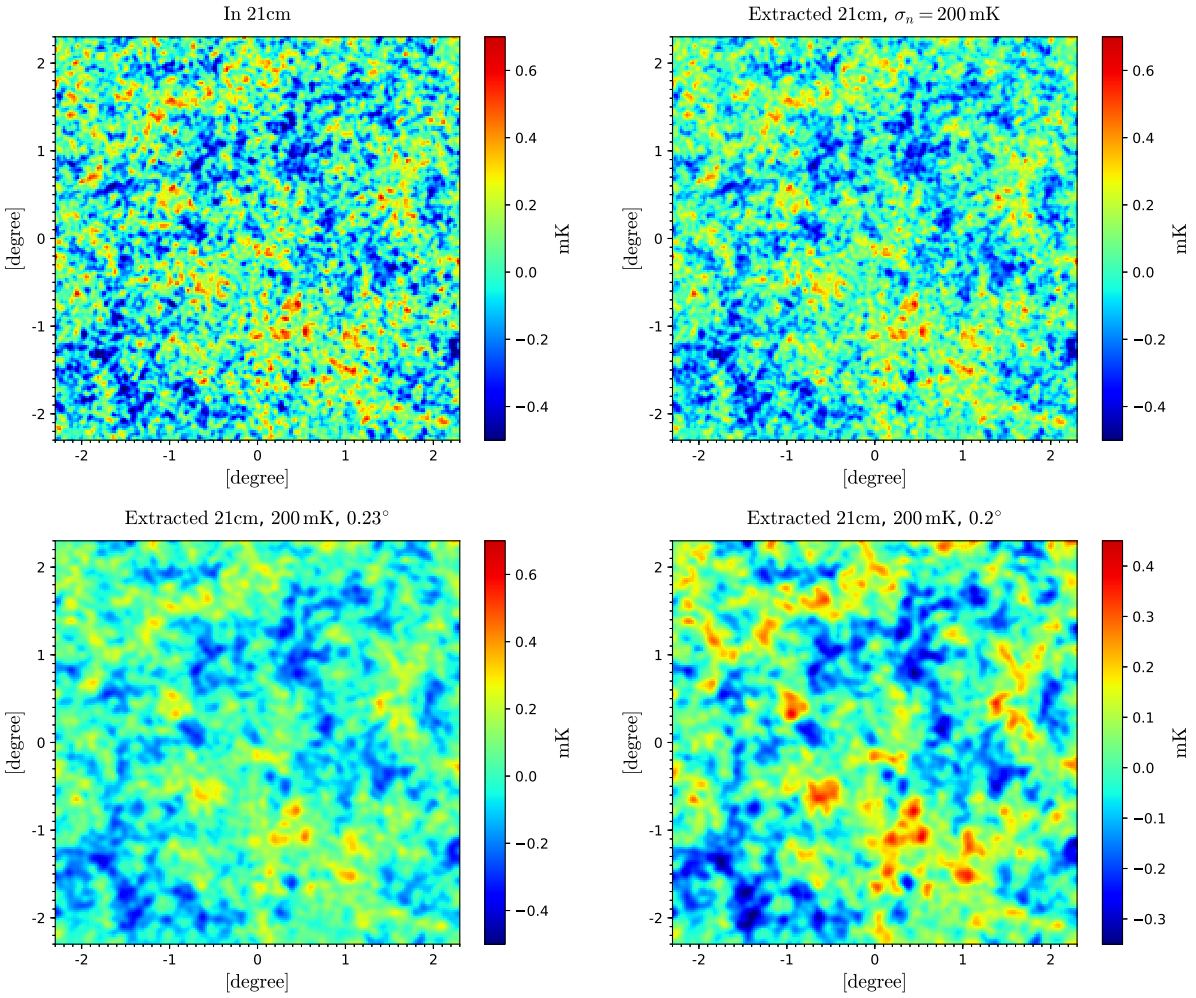

Fig. 9 Effect of inaccurate beam on map reconstruction. Here we assume the real beam size is 0.25°. *Top Left*: input 21 cm map; *Top Right*: reconstructed 21 cm map from noise of 200 mK, with the correct beam size of 0.25°; *Bottom Left*: reconstruction with the incorrect beam width of 0.23°; *Bottom Right*: reconstruction with the incorrect beam width of 0.20°.

is still very similar. In the real world, of course, deviation from the beam might be more irregular and complicated, but the overall effect would be losing the details below the beam resolution while retaining the larger overall structures.

4 DISCUSSION AND CONCLUSIONS

A 3D cosmological neutral hydrogen survey over a large fraction of the sky is an efficient way to study our Universe. A number of instruments have been developed or are being designed for such surveys. However, a great challenge is that both the foreground radiation and noise are several orders of magnitude larger than the 21 cm signal. To extract the cosmological 21 cm signal from the data collected from such instruments, an efficient extraction method is required.

This paper is an exploratory study of this issue using the Wiener filter, which is widely utilized in the field of signal processing. We have taken as an example the analysis of data processing for a mid-redshift experiment, which is aimed at measuring the dark energy equation of state by using the BAO features in the large scale structure. However, the method is also applicable for the EoR experiments. Assuming that the data have been preprocessed and an image cube has been produced, we used a two step procedure to extract the 21 cm signal. We first subtract the foreground by removing the smooth component in the frequency spectrum along each LoS. Previously, Liu & Tegmark (2012) applied the Wiener filter method to extract the foreground from the 21 cm experiment, but they are mostly concerned with the frequency spectrum, which is applicable to the 21 cm global spectrum experiment, or to one LoS for the 21 cm intensity mapping experiment, corresponding to this first step. However, we then go one step further, extracting the 21 cm signal by applying the Wiener filter on the 2D angular space. Our simulation shows that the 21 cm signal could be recovered with good precision. In actual data analysis, the power spectrum of the 21 cm signal is not precisely known, but from other cosmological observations an approximate value could be inferred. Starting from the approximate value, one can apply the filter iteratively to improve the estimate.

In the present study we have made a number of simplifying assumptions. In an actual experiment, the beam shape is more complicated, frequency-dependent and only known to a limited precision, the calibration procedure may introduce additional errors, and the noise may be non-thermal and have more complicated statistical properties. All of these factors may affect the extraction of the 21 cm signal. To overcome these problems, one needs to consider the specific experiment. Nevertheless, the Wiener filtering may provide a very useful tool for 21 cm data analysis.

Acknowledgements This research is supported by the Ministry of Science and Technology (2016YFE0100300), the National Natural Science Foundation of China (Grant Nos. 11473044, U1501501, U1631118 and 11633004), and the Chinese Academy of Sciences (QYZDJ-SSW-SLH017). F.Q. Wu also acknowledges support by the CSC Cai Yuanpei grant.

References

Bandura, K., Addison, G. E., Amiri, M., et al. 2014, in Proc. SPIE, 9145, Ground-based and Airborne Telescopes V, 914522

Battye, R. A., Browne, I. W. A., Dickinson, C., et al. 2013, MNRAS, 434, 1239

Chang, T.-C., Pen, U.-L., Bandura, K., & Peterson, J. B. 2010, Nature, 466, 463

Chang, T.-C., Pen, U.-L., Peterson, J. B., & McDonald, P. 2008, Physical Review Letters, 100, 091303

Chapman, E., Abdalla, F. B., Harker, G., et al. 2012, MNRAS, 423, 2518

Chen, X. 2012, in International Journal of Modern Physics Conference Series, 12, 256

Ciardi, B., & Madau, P. 2003, ApJ, 596, 1

de Oliveira-Costa, A., Tegmark, M., Gaensler, B. M., et al. 2008, MNRAS, 388, 247

DeBoer, D. R., Parsons, A. R., Aguirre, J. E., et al. 2017, PASP, 129, 045001

Dickinson, C. 2014, arXiv:1405.7936

Gleser, L., Nusser, A., & Benson, A. J. 2008, MNRAS, 391, 383

Huynh, M., & Lazio, J. 2013, arXiv:1311.4288

Jelić, V., Zaroubi, S., Labropoulos, P., et al. 2008, MNRAS, 389, 1319

Liu, A., & Tegmark, M. 2012, MNRAS, 419, 3491

Loeb, A., & Zaldarriaga, M. 2004, Physical Review Letters, 92, 211301

Madau, P., Meiksin, A., & Rees, M. J. 1997, ApJ, 475, 429

Mao, Y., Tegmark, M., McQuinn, M., Zaldarriaga, M., & Zahn, O. 2008, Phys. Rev. D, 78, 023529

Masui, K. W., Switzer, E. R., Banavar, N., et al. 2013, ApJ, 763, L20

Nan, R., Li, D., Jin, C., et al. 2011, International Journal of Modern Physics D, 20, 989
Newburgh, L. B., Bandura, K., Bucher, M. A., et al. 2016, in Proc. SPIE, 9906, Ground-based and Airborne Telescopes VI, 99065X (arXiv:1607.02059)
Paciga, G., Chang, T.-C., Gupta, Y., et al. 2011, MNRAS, 413, 1174
Parsons, A. R., Backer, D. C., Foster, G. S., et al. 2010, AJ, 139, 1468
Planck Collaboration, Ade, P. A. R., Aghanim, N., et al. 2016, A&A, 594, A13
Reich, P., & Reich, W. 1988, A&AS, 74, 7
Santos, M. G., Cooray, A., & Knox, L. 2005, ApJ, 625, 575
Shaver, P. A., Windhorst, R. A., Madau, P., & de Bruyn, A. G. 1999, A&A, 345, 380
Switzer, E. R., Masui, K. W., Bandura, K., et al. 2013, MNRAS, 434, L46
Tegmark, M. 1997, ApJ, 480, L87
Testori, J. C., Reich, P., Bava, J. A., et al. 2001, A&A, 368, 1123
Tingay, S. J., Goeke, R., Bowman, J. D., et al. 2013, PASA, 30, e007
van Haarlem, M. P., Wise, M. W., Gunst, A. W., et al. 2013, A&A, 556, A2
Wang, X., Tegmark, M., Santos, M. G., & Knox, L. 2006, ApJ, 650, 529
Wolz, L., Abdalla, F. B., Blake, C., et al. 2014, MNRAS, 441, 3271
Xu, Y., Wang, X., & Chen, X. 2015, ApJ, 798, 40
Zhang, J., Ansari, R., Chen, X., et al. 2016a, MNRAS, 461, 1950
Zhang, J., Zuo, S.-F., Ansari, R., et al. 2016b, RAA (Research in Astronomy and Astrophysics), 16, 158
Zheng, H., Tegmark, M., Dillon, J. S., et al. 2017, MNRAS, 464, 3486
Zheng, Q., Wu, X.-P., Johnston-Hollitt, M., Gu, J.-h., & Xu, H. 2016, ApJ, 832, 190
Zuo, S., Chen, X., Ansari, R., & Lu, Y. 2018, arXiv:1801.04082